

Fine-Grained Entity Segmentation

Lu Qi^{1*}, Jason Kuen^{2*}, Weidong Guo^{3*}, Tiancheng Shen⁴, Jiuxiang Gu², Wenbo Li⁴,
 Jiaya Jia⁴, Zhe Lin², Ming-Hsuan Yang¹

¹The University of California, Merced

²Adobe Research

³QQ Browser Lab, Tencent

⁴The Chinese University of Hong Kong

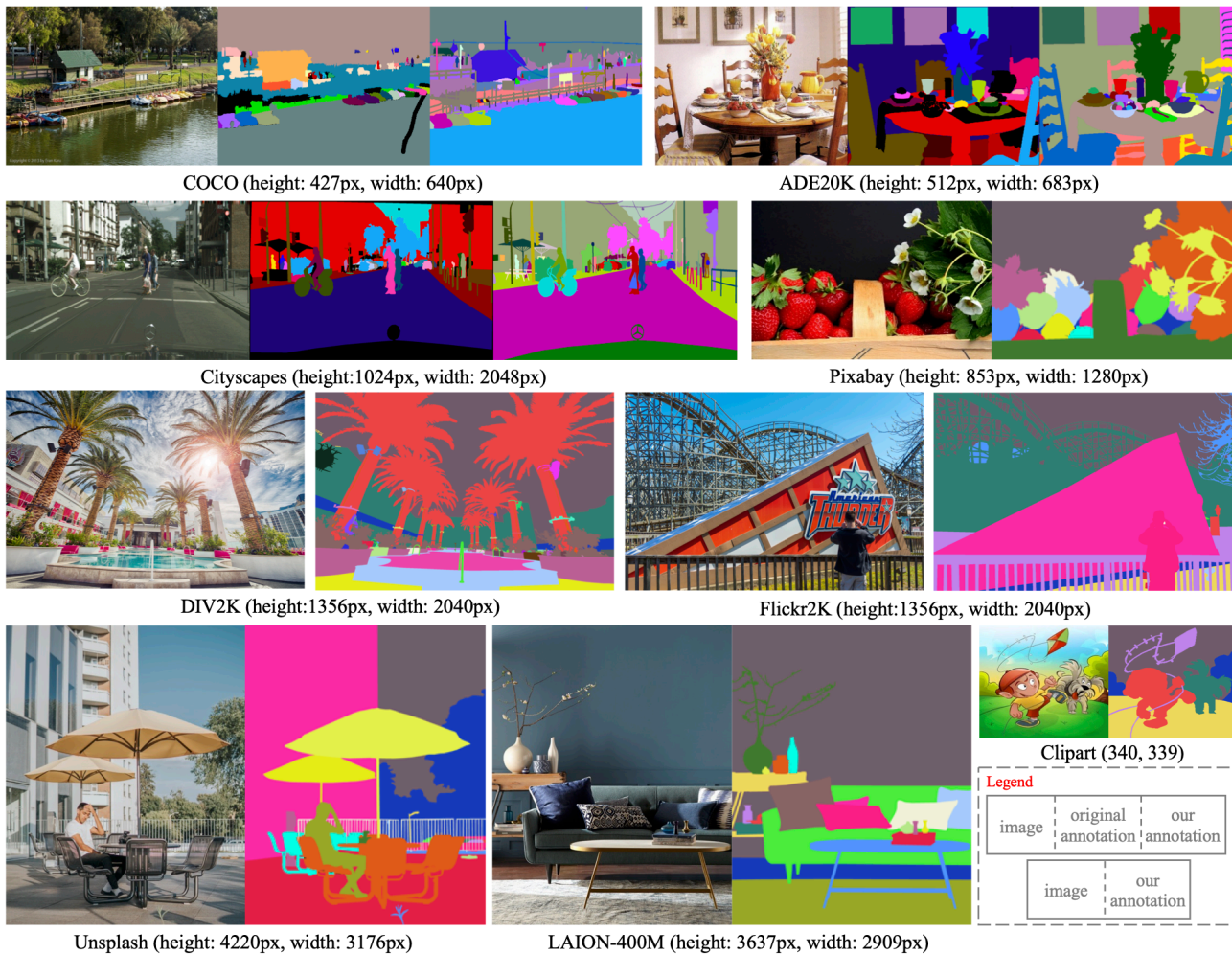


Figure 1: Fine-grained entity segmentation mask annotations for low-resolution and high-resolution images collected from existing datasets and Internet. For the images collected from COCO [32], ADE20K [61] and Cityscapes [11], we provide a visual comparison between their original and our annotations in the middle and rightmost sub-figures. For existing datasets, the areas in black color are unannotated regions. To meet the paper file size requirement, here we only include downsampled RGB and mask images that may have some quality degradation.

Abstract

In dense image segmentation tasks (e.g., semantic, panoptic), existing methods can hardly generalize well to unseen image domains, predefined classes, and image resolution & quality variations. Motivated by these observations, we construct a large-scale entity segmentation dataset to explore fine-grained entity segmentation, with a strong focus on open-world and high-quality dense segmentation. The dataset contains images spanning diverse image domains and resolutions, along with high-quality mask annotations for training and testing. Given the high-quality and -resolution nature of the dataset, we propose CropFormer for high-quality segmentation, which can improve mask prediction using high-res image crops that provide more fine-grained image details than the full image. CropFormer is the first query-based Transformer architecture that can effectively ensemble mask predictions from multiple image crops, by learning queries that can associate the same entities across the full image and its crop. With CropFormer, we achieve a significant AP gain of 1.9 on the challenging fine-grained entity segmentation task. The dataset and code will be released at <http://luqi.info/entityv2.github.io/>.

1. Introduction

Dense image segmentation is an important topic in computer vision with a wide range of applications such as autonomous driving [40], robotics [46], video surveillance [38], and image editing tools. Recently, entity segmentation [42] has been introduced as a promising dense instance-aware approach for tackling generalization issues caused by narrow image domains and/or predefined class sets in existing panoptic [22, 21, 56, 28, 4] and semantic [36, 57, 7, 8, 58, 19, 33] segmentation tasks. Although the early method [42] shows some promising results, it merely borrows existing panoptic segmentation datasets to demonstrate the feasibility and benefits of the entity segmentation. However, existing panoptic segmentation datasets (e.g. COCO [32], Cityscapes [11], ADE20K [61]) suffer from the same issues that entity segmentation [42] aims to avoid, since those datasets are collected and annotated with panoptic segmentation task requirements in mind.

Motivated by the above-discussed observations, we propose a new large-scale, high-quality dataset for entity segmentation. Our dataset has three important characteristics: 1) we collect about 33,227 images from public datasets and the Internet. These images cover various domains such as landscapes, outdoor/indoor scenes, cartoons, graphical illustrations, and computer games; 2) the annotations are open-world without any predefined class restrictions and

densely cover the entire images; 3) we elevate the segmentation quality objective of entity segmentation [42] to the next level by annotating high-quality masks with fine-grained details on high-resolution images. There are over 70% images that have high image resolutions, spanning from 2K to 15K, with significantly more accurate boundary annotations compared to existing panoptic datasets. As shown in Figure 1, our diversified dataset provides fine-grained segmentation masks on high-res images, along with open-world annotations on low-res images from public datasets.

In addition to the fine-grained segmentation dataset, we evaluate widely-used segmentation models on our dataset. The high-resolution images and ground-truth (GT) masks in our dataset bring new challenges to existing segmentation approaches. The segmentation quality is sacrificed if we downsample the images and GT masks to 800px resolution during training (standard practice in Detectron2 [54] or MMDetection[5]), whereas using a larger input resolution causes out of memory issues on GPUs.

We propose CropFormer to tackle the high-resolution segmentation problem using a divide-and-conquer approach. CropFormer generates mask predictions from both the full image and its high-resolution crops, and then ensemble their mask predictions. During training, we randomly select one of the predefined 4 corner crops to pair with the full image. During inference, we apply CropFormer to all corner crops to ensemble their mask prediction results. The key strength of CropFormer is to utilize the same queries to associate the same entities across the full image and its crops, allowing us to ensemble their mask predictions during inference to obtain stronger final results. Our work is the first to overcome the limitation of existing query-based panoptic/instance segmentation methods [10, 9, 29] being not compatible with test-time augmentation (TTA), due to unassociated queries across different image views¹.

The main contributions of this work are:

- We collect a large-scale, high-quality entity segmentation dataset with images collected from various domains with different resolutions and high-quality masks. Our dataset enables the evaluation of the generalization and robustness capabilities of segmentation models in a unified manner, through an open-world, domain-diverse, and high-resolution setting.
- We benchmark several segmentation models on the new dataset. We find that the traditional training setting cannot fit well to our dataset where over 70% are very high in resolution. We propose CropFormer to associate the same entities in different crops by the same

¹That is due to the use of Hungarian algorithm that performs unconstrained matching between queries and ground-truths, causing the same ground-truths across different image views to be represented by unmatched queries. We show some cases in our supplementary file.

queries. To the best of our knowledge, we are the first to achieve ensemble-based prediction using different image crops in query-based segmentation frameworks.

- Extensive experiments and in-depth analysis show the merits of the proposed model and dataset, which will facilitate future research in this field.

2. Related Work

Image Segmentation Dataset Numerous datasets have been proposed for semantic, instance, and panoptic segmentation, *e.g.*, Microsoft COCO [32], ADE20K [61], KITTI [14], LVIS [16], PASCAL-VOC [13], Open-Images [24], Cityscapes [11], *etc.* In addition, there are some datasets designed for specific scenarios, such as amodal segmentation (COCO-Amodal [62], KINS [40]), human segmentation (CelebAMask-HQ [25], LIP [15], MHP [59]) and domain adaptation (Synscapes [52], GTA5 [43]). Despite significant contributions from these datasets, it is of great interest to fulfill the needs of real-world applications with high-quality images with large diversity. For example, a segmentation model should be robust to high-resolution images from different domains. Meanwhile, models should be able to segment unseen objects in the open-world setting. Most relevant to our work is the ADE20K dataset [61], which has large-scale open-vocabulary categories. However, the collected images in ADE20K are of low resolution and from narrowed domains. In our dataset, we collect the images from multiple image domains, including indoor, outdoor, street scenes, and even cartoon and remote image domains. In addition, over 80% of the images resolution fall within the high-resolution range of 2000px and 8000 px. Compared to the ADE20K [60] and LVIS [16] dataset with a predefined category list, our annotation process is different. We first conduct class-agnostic mask annotation on each entity. After that, the category information is then labeled in an open-vocabulary manner.

Scene Parsing Methods Scene parsing methods are mainly developed by convolution-based dense prediction or transformer-based query prediction. The method based on convolution-based dense prediction often uses explicit localization information like bounding box proposals or pixel position for pixel-level mask prediction. These approaches include FCN [36], DeepLab [6], PSPNet [57], Mask R-CNN [17], PANet [34], SOLO [50], CondInst [47], PanopticFPN [21], and PanopticFCN [27]. Motivated by the success of transformers DETR [4] for detection tasks [30, 31, 12, 41], numerous methods, *e.g.*, Max-Deeplab [49] and Mask2Former [10], directly predict segmentation masks without the guidance of bounding boxes. The key to these methods is to use learnable queries to model the implicit location of the potential instance area. Although query-based

methods are effective, they cannot benefit from TTA which is commonly used to boost the accuracy of convolution-based methods. Specifically, it is challenging for a query-based method to ensemble multiple results from augmented image views, due to the lack of exact location for queries. Motivated by video-level Mask2Former, we endow the queries with ability to connect the same entities among different image views. As such, our approach can enhance high-resolution image segmentation by combining results from full image and local crops.

3. EntitySeg Dataset

The EntitySeg dataset contains 33,227 images with high-quality mask annotations. Compared with existing datasets, there are three distinct properties in EntitySeg. First, 71.25% and 86.23% of the images are of high resolution with at least 2000px×2000px and 1000px×1000px which is more consistent with current digital imaging trends. Second, our dataset is open-world and is not limited to predefined classes. We regard every semantically-coherent region in the images as an entity, even if it is a blurred region or it cannot be semantically recognized easily. Third, the mask annotation along the boundaries are more accurate than existing datasets, as shown in Figure 1. In the following, we describe our EntitySeg dataset and provide comprehensive analysis.

3.1. Image Collection

Inspired by the collection criterion of COCO [32], we collect most non-iconic images with more contextual information and non-canonical viewpoints. In addition, the image domains should be as diversified as possible to guarantee substantial domain diversity. Therefore, the image sources of our dataset include several public datasets and the Internet where the images permitted for academic research use. For public dataset sources, we select part of the images from COCO [32], ADE20K [61], Pascal VOC [13], Cityscapes [11], Mapillary Vistas [39], ImageNet [23], Open Images [24], DIV2K [3], Flickr2K [51], Clipart [20], Comic [20], DOTA [55] and some computer game screenshots from Synscapes [52] and GTA5 [43]. From the Internet, we crawled mainly high-resolution images from Pixabay [1], Unsplash [2], and LAION-400M [45]. In Figure 2(c), we show the distribution of image sources in our dataset and see that most of the images are from high-resolution sources like Pixabay, Unsplash, and LAION-400M. In Figure 2(a), our dataset has more high-resolution images whose resolutions are normally distributed in the resolution range between 0px to 15,000px, whereas all the images of ADE20K [61] and COCO [32] are under 1000px.

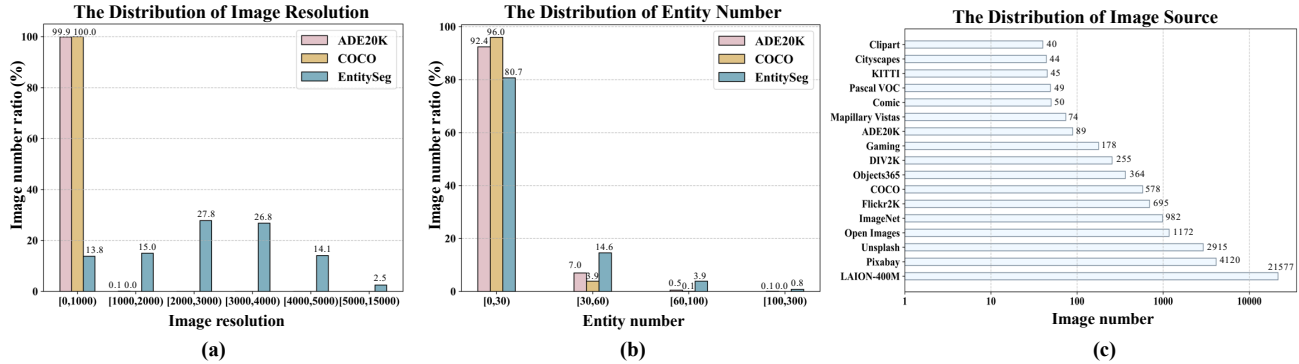


Figure 2: Sub-figures (a) and (b) illustrate the distributions of image resolutions and average number of entities among ADE20K, COCO, and EntitySeg. Sub-figure (c) shows the distribution of image sources we collected EntitySeg images from.

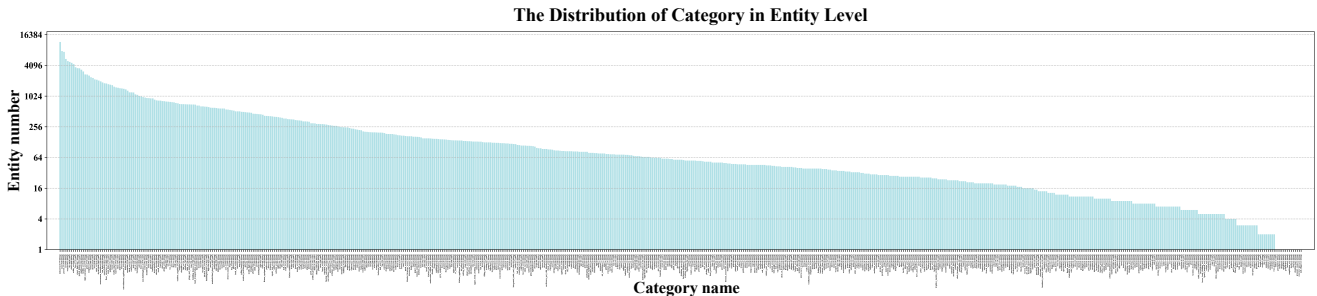


Figure 3: The class distribution of the EntitySeg dataset. Here we mention if a class belongs to *thing* or *stuff*. Please zoom in on the x-axis of the figure to look at the class names.

3.2. Image Annotation

The annotation process for our dataset mainly consists of three steps. For an image, we firstly annotate all entities with class-agnostic pixel-level masks where each mask has no overlaps with others. After that, each mask is annotated with a class label based on a large vocabulary class set, which is not fixed but updated continuously over time. There are two special considerations here. On one hand, we annotate the entity as ‘unknown’ or ‘blurred’ if it cannot be name easily or severely blurred. On the other hand, the entity is annotated as a ‘*supercategory_other*’ if we merely know it is a *supercategory* but unable to identify its fine-grained class. Our annotation process is the direct opposite of those of the popular segmentation datasets like COCO [32] and ADE20K [60], where class sets are predefined first before annotating masks based on the predefined classes. In Table 2, it shows that our dataset has a greater proportion of covered image areas and number of masks on average than COCO- and ADE20K-Panoptic. This is by virtue of our novel annotation process that allows us to take into account all the semantically-coherent regions, and then assign class labels to them. In addition, our annotation process is more similar to the the human vision system. This

	ann ₁	ann ₂	ann ₃
ann ₁	-	-	-
ann ₂	90.6	-	-
ann ₃	91.2	92.1	-

(a)

	ann ₁	ann ₂	ann ₃
ann ₁	-	-	-
ann ₂	95.4	-	-
ann ₃	94.8	95.2	-

(b)

Table 1: Annotation consistency of class-agnostic localization and class-aware categories among annotators.

is consistent with human vision system that is inherently class-agnostic and is able to recognize entities without understanding its use and purpose, as explained by Marr [37].

Annotation consistency is a crucial aspect of any human-labeled dataset since it tells whether the annotation task is well-defined and reasonable. We randomly selected 500 images from our dataset (1.5% of the entire dataset) and asked another two annotators to separately annotate them again after four months. Table 1(a) shows the class-agnostic mask mAP in the first step of the annotation process compared to those of the other two annotators. We use one as ground truth, and another one as prediction results. In addition, we evaluate the category consistency by accuracy (ACC) under the same mask annotations in Table 1(b). These two tables indicate our dataset has a high degree of annotation consistency both in the mask and category labeling stages.

Dataset	ImageRes (avg)↑	EntityNum (avg)↑	EntityNum (max)↑	Entity Complexity↓	Entity Simplicity↓	Valid Area↑
COCO	522.5	11.2	95	0.758	0.581	0.891
ADE20K	461.3	13.6	255	0.802	0.606	0.914
EntitySeg	2700.7	18.1	236	0.719	0.538	0.999

Table 2: The statistical comparisons between COCO [32], ADE20K [61] and EntitySeg. ‘ImageRes (avg)’, ‘EntityNum (avg)’, ‘Valid Area’, ‘Entity Complexity’, and ‘Entity Simplicity’ refer to the average value of image resolution size, entity numbers per image, valid area ratio per image, average entity complexity and simplicity respectively. ‘EntityNum (max)’ means the maximum per-image number of entities within each dataset.

3.3. Dataset Statistics

In the EntitySeg dataset, we annotate all images at the entity level, regardless of whether they belong to thing or stuff in previous datasets. As shown in Figure 1, we show some low- and high-resolution photos and their mask annotations to highlight our high-quality pixel-level annotation quality. For example, one can zoom in on the Unsplash image to see how fine-grained the railing’s mask is.

We present the quantitative comparison among our dataset, COCO-Panoptic [32], and ADE20K-Panoptic [61] in Table 2. In the EntitySeg dataset, each image has 18.1 entities on average, which is more than 11.2 and 13.6 entities in COCO and ADE20K. The detailed comparison among those three datasets on the distribution of entity number is shown in Figure 2(b). Furthermore, the shapes of entities in our dataset are more complex than those COCO [32] and ADE20K [61] as represented by the columns ‘Entity Complexity’ and ‘Entity Simplicity’ of Table 2 where an entity with a large convexity and simplicity value means it is a simple shape (and both metrics achieve their maximum value of 1.0 for a circle [62]). More details about how complexity and simplicity are calculated can be found in the supplementary material.

Class-Aware Annotation We select a subset of 11,580 images from the entire dataset for class labeling, which forms the EntityClass dataset. In our annotation process, the class is labeled in an open-vocabulary and free-form manner, then the class set is continually expanded. After the class annotation process, we organize and merge the annotated classes according to Word-Tree [44]. This results in 535 thing and 109 stuff classes for EntityClass. Figure 3 shows the class frequency distribution which follows Zipf’s law, resembling existing datasets like COCO [32] and ADE20K [61].

4. Method

Preliminary work on entity segmentation [42] shows that instance segmentation frameworks are generally applicable to entity segmentation. In this work, we build our

CropFormer on top of Mask2Former [10], which is the state-of-the-art query-based image segmentation method. In the following, we first revisit our baseline framework Mask2Former [10]. Based on this baseline framework, we then introduce the proposed CropFormer that enables queries to associate the same entity cross various image views. At last, we describe the training and inference processes of our framework.

4.1. Mask2Former Preliminaries

Mask2Former [10] is a universal Transformer-based framework for image or video instance segmentation. Given an input, Mask2Former uses a Transformer decoder to decode N number of K -dimensional queries $\mathbf{Q} \in \mathbb{R}^{N \times K}$ to generate embeddings $\mathbf{E} \in \mathbb{R}^{N \times 1 \times 1 \times 1 \times K}$ to predict N segmentation masks, where the 2nd, 3rd, and 4th dimensions of \mathbf{E} correspond to temporal (T), output height (H), and output width (W) dimensions respectively. When applying the image-level Mask2Former to an image input, \mathbf{E} is broadcasted along spatial dimensions to the shape of $N \times 1 \times H \times W \times K$. Alternatively, when applying video-level Mask2Former to a video input, \mathbf{E} is broadcasted to the shape of $N \times T \times H \times W \times K$. Note that in video-level Mask2Former, \mathbf{E} is further broadcasted along the both temporal and spatial dimensions, enabling Mask2Former to utilize the same embeddings to represent the same visual instances across different frames consistently.

4.2. CropFormer

We introduce a new architecture called CropFormer combines the strengths of both image-level and video-level Mask2Formers along with high-resolution crop inputs to improve the quality of fine-grained entity segmentation. In the following, we provide the details of several key components of CropFormer.

Crop Dataloader In CropFormer, the crop dataloader is designed to generate a batch of images that simultaneously include the full images and their corresponding crops. There are two steps in our dataloader: *crop* and *resize*. At first, we augment the full image I^o with a crop that is part of the full image. The crop is randomly extracted from one of the fixed image corners: upper-left, upper-right, bottom-left, bottom-right. The crop size is controlled by a fixed ratio hyperparameter $\delta \in \mathbb{R}$ relative to the full image size. Second, we resize both the full image and crop to the same size. In this way, we construct an input batch $\mathbf{I} \in \mathbb{R}^{N \times 2 \times H_1 \times W_1 \times 3}$ with 2 elements (full image & 1 crop) along the temporal dimension. Compared to the full image, corner crops preserve more image details and local information useful for fine-grained segmentation. Given dataloader Γ , we define the data preprocessing as

$$\mathbf{I} = \{I^o, I^c\} = \Gamma(I^o, \delta), \quad (1)$$

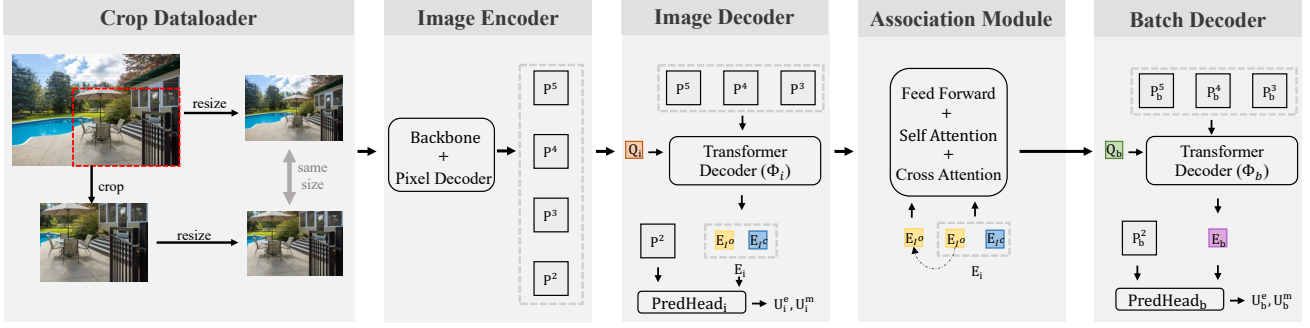


Figure 4: Framework of the proposed CropFormer. The box in red color indicates our cropped region randomly sampled from four fixed image corners.

where I^c is the crop. Compared to the strategy of random cropping in state-of-the-art video instance segmentation methods SeqFormer [53] and VITA [18], we adopt a stricter fixed crop strategy to keep training and inference consistent. This provides a strong inference efficiency because it is sufficient to evaluate a fixed number of crops during inference, rather than many random crops.

Image Encoder and Decoder Based on learnable image-level queries $\mathbf{Q}_i \in \mathbb{R}^{N \times K}$, we use image encoder Θ and decoder Φ_i to generate image-level embeddings $\mathbf{E}_i \in \mathbb{R}^{N \times 2 \times 1 \times 1 \times K}$ for the full input image and its crop. For the image encoder and decoder, we directly adopt the ones in standard image-level Mask2Former [10] and do not modify their structures or designs. \mathbf{E}_i is obtained as follows:

$$\mathbf{E}_i = \Phi_i(\mathbf{Q}_i, \Theta(\mathbf{I})), \quad (2)$$

\mathbf{E}_i is used for image-level entityness prediction and pixel-level prediction using image-level pyramid features \mathbf{P}_i^h (derived from the image encoder including backbone and pixel decoder) and a prediction head as:

$$\mathbf{U}_i^e, \mathbf{U}_i^m = \text{PredHead}_i(\mathbf{E}_i, \mathbf{P}_i^h), \quad (3)$$

where \mathbf{U}_i^e and \mathbf{U}_i^m are the entityness prediction and pixel-level mask outputs. Here, we employ i subscript to differentiate image-level embeddings and mask outputs from those of the association module.

Association Module Similar to video-level Mask2Former [9], the association module aims to generate batch queries \mathbf{Q}_b that are fully shared by the full image and its crop to represent the same entities consistently. Instead of treating \mathbf{Q}_b as learnable network parameters, here we generate \mathbf{Q}_b directly from $\mathbf{E}_i = \{\mathbf{E}_{I^o}, \mathbf{E}_{I^c}\}$, considering that \mathbf{E}_i already contains strong segmentation features. In particular, we use a Transformer architecture with cross attention (XAtt), self-attention (SAAtt), and feedforward network (FFN) to obtain \mathbf{Q}_b :

$$\mathbf{Q}_b = \text{FFN}(\text{SAAtt}(\text{XAtt}(\underbrace{f_q(\mathbf{E}_{I^o})}_{\text{query}}, \underbrace{f_k(\mathbf{E}_i)}_{\text{key}}, \underbrace{f_v(\mathbf{E}_i)}_{\text{value}}))), \quad (4)$$

where $f_{\{q,k,v\}}$ are linear transformations. Since the full image is more crucial to entity segmentation than its crop, we take the image-level embeddings of the full image \mathbf{E}_{I^o} as the *query*, while treating all the image-level embeddings \mathbf{E}_i as *key* and *value*. This design is similar to the cross-attention of original Transformer [48] and SelfDoc [26].

Batch Decoder Given $\mathbf{Q}_b \in \mathbb{R}^{N \times 1 \times 1 \times 1 \times K}$, we obtain batch embeddings $\mathbf{E}_b \in \mathbb{R}^{N \times 1 \times 1 \times 1 \times K}$:

$$\mathbf{E}_b = \Phi_b(\mathbf{Q}_b, \Theta(\mathbf{I})), \quad (5)$$

Similar to video-level Mask2Former, the full image and its crop can be seen as 2 video frames. Thus, we broadcast \mathbf{E}_b to the shape of $N \times 2 \times 1 \times 1 \times K$ to share it between the full image and its crop. \mathbf{E}_b and batch-level pyramid features $\mathbf{P}_b^h \in \mathbb{R}^{1 \times 2 \times H^h \times W^h}$ (reshaped from $\mathbf{P}_i^h \in \mathbb{R}^{2 \times 1 \times H^h \times W^h}$) are used for batch-level mask classification and pixel-wise prediction:

$$\mathbf{U}_b^e, \mathbf{U}_b^m = \text{PredHead}_b(\mathbf{E}_b, \mathbf{P}_b^h), \quad (6)$$

The main difference between \mathbf{P}_b^h and \mathbf{P}_i^h is whether we regard the images (including full image and crop) as two images stacked along the batch dimension or as two video frames stacked along the temporal dimension.

4.3. Training and Inference

Training During training, we employ two separate losses \mathcal{L}_i and \mathcal{L}_b for image- and batch-level predictions, with respect to ground truth \mathbf{G} . The main difference between the two lies in whether the same entities in full image and crop are tied to the same queries. Our overall training loss is:

$$\mathcal{L} = \sum_{k \in \{1, b\}} \mathcal{L}_k^{\text{ce}}(\mathbf{U}_k^e, \mathbf{G}_k^e) + \sum_{k \in \{1, b\}} \mathcal{L}_k^{\text{bce}}(\mathbf{U}_k^m, \mathbf{G}_k^m) + \sum_{k \in \{1, b\}} \mathcal{L}_k^{\text{dice}}(\mathbf{U}_k^m, \mathbf{G}_k^m), \quad (7)$$

where $\mathcal{L}_i^{\text{ce}}$ and $\mathcal{L}_b^{\text{ce}}$ denote binary cross-entropy loss for image- and batch-level entityness prediction. Similarly,

$\mathcal{L}_i^{\text{bce}}$, $\mathcal{L}_b^{\text{bce}}$, $\mathcal{L}_i^{\text{dice}}$ and $\mathcal{L}_b^{\text{dice}}$ denote the binary cross-entropy and dice loss for image- and batch-level mask prediction.

Inference An ensemble of predictions from multiple image views (or TTA) is a common practice in deep learning, but has never been explored in the context of query-based segmentation architectures [10, 9, 29]. The reason is that the queries are implicitly tied to certain spatial locations of the input and thus unrobust to transformations (*e.g.*, scaling, cropping), which we show in our supplementary file. As a result, the same entity across different image views are likely predicted by different queries. Therefore, it is not possible to ensemble the results of unmatched image views using previous query-based methods. However, with CropFormer, during inference, we can easily ensemble the batch-level prediction results. This is because the same entities between the full image and its crop are represented by the same queries, by virtue of the association module. For the final segmentation output, we ensemble the per-pixel mask predictions obtained from the full image and every crop of the 4 corners (Sec. 4.2). The confidence score of each entity comes from the batch-level entityness prediction score.

5. Experiments

We conduct our main experiments on our proposed EntitySeg Dataset. We first benchmark our dataset in several segmentation tasks, including entity, instance, semantic and panoptic segmentation. Then, we ablate our proposed CropFormer to demonstrate its effectiveness.

For the training set, we use the same hyper-parameters of the COCO training except for the training iterations and learning rate steps considering the dataset size difference. Our EntitySeg dataset defines $1\times$ training schedule as 34,375 iterations and decays learning rate after 30,525 and 33,138 iterations. $N\times$ training schedule indicates that the number of iterations and learning rate decay schedule are adjusted by a factor of N . Given the EntityClass dataset has only one-third image numbers of the EntitySeg dataset, the $1\times$ training schedule is sufficient to obtain the best performance on class-aware segmentation tasks. We leave out some details and some experiments due to paper length limitation. Please refer to our supplementary file for more information.

5.1. Entity Dataset Benchmark

Entity Segmentation We divide the EntitySeg dataset into train and test sets, which have 31,913 and 1,314 images. To obtain a less-biased dataset split, we constructed 20 random dataset splits. We selected the dataset split that is statistically closest to the all 20 splits in terms of entity segmentation accuracy, as detailed in the supplementary file. Furthermore, we use class-agnostic metric AP^c [42] with a strict non-overlapping mask constraint to evaluate the entity segmentation task.

Model	Backbone	Iteration	Pretrain	AP^c	AP_{50}^c	AP_{75}^c
Mask-RCNN [17]	Swin-T	$1\times$	ImageNet	24.9	45.8	24.1
			COCO-E	28.4	49.2	28.1
EntityFramework [42]	Swin-T	$1\times$	ImageNet	26.0	42.8	25.7
			COCO-E	29.9	47.6	30.1
Mask2Former [10]	Swin-T	$1\times$	ImageNet	33.2	50.2	33.1
			COCO-E	39.5	56.9	40.2
		$2\times$	COCO-E	40.2	57.6	41.1
		$3\times$	COCO-E	40.9	58.1	41.6
	$4\times$	COCO-E	40.9	57.9	41.9	
	Swin-L	$3\times$	COCO-E	46.2	63.7	47.5

Table 3: Entity segmentation benchmark in Entity Dataset. The column of ‘Pretrain’ indicates the pretraining weights we used where the ‘ImageNet’ is ImageNet pretraining and ‘COCO-E’ refers to pretraining on COCO dataset that has been converted to class-agnostic entity segmentation format [42].

Table 3 shows the benchmark of our dataset with Mask-RCNN [17], EntityFramework [42], Mask2Former [10]. The first two methods are convolution-based dense prediction methods, whereas the last is a transformer-based query prediction method. In this table, the transformer-based Mask2Former is better than the other two convolution-based methods, demonstrating the advantage of transformer-based methods on high-quality mask generation. Moreover, the COCO-E pretrained weights can further boost entity segmentation performance. We also explored the optimal training iterations needed by Mask2Former and found that it performs the best with $3\times$ training schedule.

Semantic Segmentation We choose 150 categories with the highest pixel-level frequency as EntitySem for semantic segmentation. EntitySem has 9,729 and 1,444 images for training and testing, respectively. In Table 4, we evaluate the two popular semantic segmentation methods DeeplabV3 [6] and Mask2Former [10] on EntitySem. Semantic segmentation performance is still related to the pre-training weights and network structure. Mask2Former with Swin-L backbone and COCO-E pretrained weights obtains the best mIoU of 50.5 on EntitySem.

Instance Segmentation We select 206 thing categories with the highest object-level frequency in the EntityClass dataset to benchmark instance segmentation. In the EntityIns, 8,993 and 1,498 images for training and testing, respectively. In Table 5, we ablate two popular instance segmentation methods including Mask-RCNN [17] and Mask2Former [10] on EntityIns. Mask2Former with Swin-L backbone and COCO-P pretrained weights the best AP of 30.3 on EntityIns.

Panoptic Segmentation Similar to EntityIns, we select 345 categories, including 274 things and 71 stuff, with the highest entity-level frequency to construct EntityPan. In EntityPan, there are 9,968 and 1,481 images for training and testing. Table 6 shows the performance of two popular panoptic segmentation methods, including PanopticFPN [21] and Mask2Former [10]. In this table, we see

Model	Backbone	Pretrain	mIoU
DeeplabV3 [7]	R-50	ImageNet	27.9
Mask2Former [10]	R-50	ImageNet	37.8
		COCO-P	43.3
	Swin-T	COCO-E	43.0
		COCO-P	45.0
	Swin-L	COCO-E	50.7
		COCO-P	50.5

Table 4: Benchmark on class-aware semantic segmentation in EntitySem Dataset. The ‘COCO-P’ and ‘COCO-E’ indicate weights trained in the COCO datasets with panoptic and entity segmentation tasks.

Model	Backbone	Pretrain	AP	AP ₅₀	AP ₇₅
Mask-RCNN [17]	R-50	ImageNet	5.0	9.3	4.9
		COCO-I	11.9	18.9	12.4
Mask2Former [10]	R-50	ImageNet	13.0	19.6	13.3
		COCO-I	20.3	29.2	21.0
	Swin-T	COCO-E	20.0	28.8	20.7
		COCO-I	22.5	32.4	23.5
		COCO-P	22.7	32.7	23.5
	Swin-L	COCO-E	28.0	39.3	29.4
		COCO-P	30.3	42.3	31.6

Table 5: Benchmark on class-aware instance segmentation in Entity Dataset. The ‘COCO-I’ indicates weights trained in the COCO datasets with instance segmentation tasks.

Model	Backbone	Pretrain	PQ	SQ	RQ
PanopticFPN [21]	R-50	ImageNet	3.6	25.8	5.5
		COCO-P	6.7	36.4	10.1
Mask2Former [10]	R-50	ImageNet	5.5	26.3	8.2
		COCO-I	9.6	39.0	14.1
	Swin-T	COCO-E	7.4	32.6	11.0
		COCO-P	9.8	38.5	14.6
	Swin-L	COCO-E	11.7	43.2	17.3
		COCO-P	13.4	48.7	19.9

Table 6: Benchmark on class-aware panoptic segmentation in Entity Dataset.

that the PQs are much lower than those of existing panoptic datasets, due to the greater variety of class labels which makes the task more challenging. In addition, current panoptic methods perform worse on EntityPan compared to existing datasets, particularly on the recognition quality (RQ) side which adversely impacts PQ.

5.2. CropFormer

We mainly ablate CropFormer on the entity segmentation task. For CropFormer, we use the same entity training setting of Mask2Former described in section 5.1. The ablation study experiments are conducted under the default $1\times$ training schedule and COCO-E pretrained weights.

Table 7 shows the overall improvement of CropFormer to the Mask2Former [10] under $1\times$ training setting. The first and second row is our baseline Mask2Former with the single-scale inference (800 and 1040 shortest side) and (1333 and 1732 longest side) for the full images, where $1040=800\times\delta$ and $1732=1333\times\delta$ with δ 0.7 in default. For the results in the third and fourth rows, we use test-time bipartite-matching to associate the same entities obtained with multi-scale images and crops. We find no improve-

Method	Decoder	AP ^e	AP ₅₀ ^e	AP ₇₅ ^e	RT (ms)
SS-Mask2Former	Image-O	39.5	56.9	40.2	637
SS-Mask2Former($\times\delta$)	Image-O	39.9	57.4	40.3	876
MS-Mask2Former	Image-O	39.2	56.3	39.5	1324
MS-Mask2Former	Batch-OC	39.3	56.4	39.7	2783
CropFormer	Image-O	39.3	56.7	39.8	637
	Batch-O	39.1	56.6	39.7	1514
	Batch-C	40.2	57.5	40.8	1507
	Batch-OC	41.0	58.4	41.9	1545

Table 7: Ablation study on the ensemble strategy on full image and four crops. The ‘Decoder’ column indicates whether we use the inference result of the full image (‘O’), four cropped patches (‘C’), or both of them (‘OC’) from the ‘Image’ or ‘Batch’ decoder. Here, the run-time (RT) is the time of network forward except the data processing and calculated on A100 GPU.

Fusion-Style	Type	AP ^e	AP ₅₀ ^e	AP ₇₅ ^e
VI-Mask2Former [10, 9]	Parallel	39.7	57.3	40.6
VITA [18]	Cascade	39.9	57.8	40.7
Ours	Cascade	41.0	58.4	41.9

Table 8: Ablation study on the fusion style between image decoder and batch decoder. ‘Type’ indicates the structure relationship between two decoders.

ments with such inference strategies. Whereas, using the crop output from CropFormer’s batch decoder achieves a significant AP^e gain as indicated by the second last row. By combining the full image and four crop outputs from CropFormer (final row), we obtain even stronger 1.5 AP^e and 1.7 AP₇₅^e gain compared to the baseline (first row).

In the following, we summarize the results from the ablation study experiments on module design and hyperparameters of CropFormer.

Other Batch Fusion Design Table 8 shows the ablation study with different fusion designs between original images and cropped patches. Directly using video-level Mask2former or VITA fusion method merely brings marginal performance gains.

CropDataloader Table 9(a) and (b) show the ablation study on the usage of crop ratio and crop type. As indicated by Table 9(a), CropFormer obtains the best performance with a crop ratio δ of 0.7. Smaller crop ratios perform worse and it might be a problem caused by queries that are not robust against drastic image transformation, which we leave for future work. Table 9(b) shows the impacts of the type of crop and the number of crops. 4 and 8 fixed crops during training and testing performs the best.

Association Module Table 9(c) shows the ablation study on the structure of the association module. There is a slight performance difference between using self-attention or a feedforward module following cross-attention.

Longer Training Schedules Table 10(a) indicates that CropFormer consistently improves over the baseline Mask2Former when we adopt $2\times/3\times$ training schedules. A

δ	AP ^c	Train	Test	AP ^c	XAtt	SAtt	FFN	AP ^c
0.5	38.5	Random	Fixed (4)	39.7	✓	○	○	40.7
0.6	40.2	Fixed (4)	Fixed (4)	41.0	✓	○	○	40.8
0.7	41.0	Fixed (4)	Fixed (8)	41.3	✓	✓	○	40.8
0.8	40.9	Fixed (8)	Fixed (8)	41.0	✓	✓	✓	41.0

(a)

(b)

(c)

Table 9: Ablation study on the usage of crop ratio δ , crop type and association module in CropFormer. In sub-table (b), ‘Random’ indicates random crops and ‘Fixed (4/8)’ indicates 4 or 8 fixed corner crops. In sub-table(c), ✓ and ○ means whether we use the module or not.

Training	Baseline	Ours	Seg-Task	Baseline	Ours
1×	39.5	41.0 (+1.5)	Entity (AP ^s)	40.9	42.8 (+1.9)
2×	40.2	42.1 (+1.9)	Semantic (mIoU)	45.0	45.6(+0.6)
3×	40.9	42.8 (+1.9)	Instance (AP)	22.7	23.2 (+0.5)
4×	40.9	42.7 (+1.8)	Panoptic (PQ)	9.8	10.4(+0.6)

(a)

(b)

Table 10: Ablation study on the longer training time and overall improvements in our CropFormer.

similar trend is observed when using Swin-L [35] backbone, which is provided in our supplementary file.

Improvement on class-aware segmentation tasks Table 10(b) shows the class-aware task performance of CropFormer with Swin-T [35] backbone and 3× training schedule. Compared to the class-agnostic entity segmentation tasks, CropFormer provides smaller gains on class-aware segmentation task, suggesting that CropFormer mainly benefits mask prediction rather than class prediction.

6. Conclusion

This paper proposes an EntitySeg dataset and a CropFormer framework for fine-grained entity segmentation, with a strong focus on open-world and high-quality dense segmentation. The EntitySeg dataset has about 33,000 images spanning diverse image domains and resolutions, along with high-quality mask annotations for training and testing. A novel CropFormer framework is proposed to take advantage of the dataset’s high-quality and -resolution characteristics, by learning batch-level queries that enables ensemble prediction from a low-res full image and its high-res crops. We hope this work will serve as a springboard for future research on open-world and high-quality image segmentation tasks.

References

[1] Pixabay. <https://pixabay.com>. Accessed: 2022-04-17. 3

[2] Unsplash. <https://unsplash.com>. Accessed: 2022-04-17. 3

[3] Eirikur Agustsson and Radu Timofte. Ntire 2017 challenge on single image super-resolution: Dataset and study. In *CVPR Workshops*, 2017. 3

[4] Nicolas Carion, Francisco Massa, Gabriel Synnaeve, Nicolas Usunier, Alexander Kirillov, and Sergey Zagoruyko. End-to-

end object detection with transformers. In *ECCV*, 2020. 2, 3

[5] Kai Chen, Jiaqi Wang, Jiangmiao Pang, Yuhang Cao, Yu Xiong, Xiaoxiao Li, Shuyang Sun, Wansen Feng, Ziwei Liu, Jiarui Xu, Zheng Zhang, Dazhi Cheng, Chenchen Zhu, Tianheng Cheng, Qijie Zhao, Buyu Li, Xin Lu, Rui Zhu, Yue Wu, Jifeng Dai, Jingdong Wang, Jianping Shi, Wanli Ouyang, Chen Change Loy, and Dahua Lin. MMDetection: Open mmlab detection toolbox and benchmark. *arXiv preprint arXiv:1906.07155*, 2019. 2

[6] Liang-Chieh Chen, George Papandreou, Iasonas Kokkinos, Kevin Murphy, and Alan L Yuille. Deeplab: Semantic image segmentation with deep convolutional nets, atrous convolution, and fully connected crfs. *PAMI*, 2017. 3, 7

[7] Liang-Chieh Chen, George Papandreou, Florian Schroff, and Hartwig Adam. Rethinking atrous convolution for semantic image segmentation. *arXiv:1706.05587*, 2017. 2, 8

[8] Liang-Chieh Chen, Yukun Zhu, George Papandreou, Florian Schroff, and Hartwig Adam. Encoder-decoder with atrous separable convolution for semantic image segmentation. In *ECCV*, 2018. 2

[9] Bowen Cheng, Anwesa Choudhuri, Ishan Misra, Alexander Kirillov, Rohit Girdhar, and Alexander G Schwing. Mask2former for video instance segmentation. *arXiv preprint arXiv:2112.10764*, 2021. 2, 6, 7, 8

[10] Bowen Cheng, Ishan Misra, Alexander G Schwing, Alexander Kirillov, and Rohit Girdhar. Masked-attention mask transformer for universal image segmentation. In *CVPR*, 2022. 2, 3, 5, 6, 7, 8

[11] Marius Cordts, Mohamed Omran, Sebastian Ramos, Timo Rehfeld, Markus Enzweiler, Rodrigo Benenson, Uwe Franke, Stefan Roth, and Bernt Schiele. The cityscapes dataset for semantic urban scene understanding. In *CVPR*, 2016. 1, 2, 3

[12] Jifeng Dai, Haozhi Qi, Yuwen Xiong, Yi Li, Guodong Zhang, Han Hu, and Yichen Wei. Deformable convolutional networks. In *ICCV*, 2017. 3

[13] Mark Everingham, Luc Van Gool, Christopher KI Williams, John Winn, and Andrew Zisserman. The pascal visual object classes (voc) challenge. *IJCV*, 2010. 3

[14] Andreas Geiger, Philip Lenz, and Raquel Urtasun. Are we ready for autonomous driving? the kitti vision benchmark suite. In *CVPR*, 2012. 3

[15] Ke Gong, Xiaodan Liang, Dongyu Zhang, Xiaohui Shen, and Liang Lin. Look into person: Self-supervised structure-sensitive learning and a new benchmark for human parsing. In *CVPR*, 2017. 3

[16] Agrim Gupta, Piotr Dollar, and Ross Girshick. Lvis: A dataset for large vocabulary instance segmentation. In *CVPR*, 2019. 3

[17] Kaiming He, Georgia Gkioxari, Piotr Dollár, and Ross Girshick. Mask r-cnn. In *ICCV*, 2017. 3, 7, 8

[18] Miran Heo, Sukjun Hwang, Seoung Wug Oh, Joon-Young Lee, and Seon Joo Kim. Vita: Video instance segmentation via object token association. In *NeurIPS*, 2022. 6, 8

[19] Zilong Huang, Xinggang Wang, Lichao Huang, Chang Huang, Yunhao Wei, and Wenyu Liu. Ccnet: Criss-cross attention for semantic segmentation. In *ICCV*, 2019. 2

- [20] Naoto Inoue, Ryosuke Furuta, Toshihiko Yamasaki, and Kiyoharu Aizawa. Cross-domain weakly-supervised object detection through progressive domain adaptation. In *CVPR*, 2018. 3
- [21] Alexander Kirillov, Ross Girshick, Kaiming He, and Piotr Dollár. Panoptic feature pyramid networks. In *CVPR*, 2019. 2, 3, 7, 8
- [22] Alexander Kirillov, Kaiming He, Ross Girshick, Carsten Rother, and Piotr Dollár. Panoptic segmentation. In *CVPR*, 2019. 2
- [23] Alex Krizhevsky, Ilya Sutskever, and Geoffrey E Hinton. Imagenet classification with deep convolutional neural networks. In *NeurIPS*, 2012. 3
- [24] Alina Kuznetsova, Hassan Rom, Neil Alldrin, Jasper Uijlings, Ivan Krasin, Jordi Pont-Tuset, Shahab Kamali, Stefan Popov, Matteo Mallocci, Alexander Kolesnikov, et al. The open images dataset v4. *International Journal of Computer Vision*, 128(7):1956–1981, 2020. 3
- [25] Cheng-Han Lee, Ziwei Liu, Lingyun Wu, and Ping Luo. Maskgan: Towards diverse and interactive facial image manipulation. In *CVPR*, 2020. 3
- [26] Peizhao Li, Jiuxiang Gu, Jason Kuen, Vlad I Morariu, Handong Zhao, Rajiv Jain, Varun Manjunatha, and Hongfu Liu. Selfdoc: Self-supervised document representation learning. In *CVPR*, pages 5652–5660, 2021. 6
- [27] Yanwei Li, Hengshuang Zhao, Xiaojuan Qi, Yukang Chen, Lu Qi, Liwei Wang, Zeming Li, Jian Sun, and Jiaya Jia. Fully convolutional networks for panoptic segmentation with point-based supervision. *TPAMI*, 2022. 3
- [28] Yanwei Li, Hengshuang Zhao, Xiaojuan Qi, Liwei Wang, Zeming Li, Jian Sun, and Jiaya Jia. Fully convolutional networks for panoptic segmentation. In *CVPR*, 2021. 2
- [29] Zhiqi Li, Wenhai Wang, Enze Xie, Zhiding Yu, Anima Anandkumar, Jose M Alvarez, Ping Luo, and Tong Lu. Panoptic segformer: Delving deeper into panoptic segmentation with transformers. In *CVPR*, pages 1280–1289, 2022. 2, 7
- [30] Tsung-Yi Lin, Piotr Dollár, Ross Girshick, Kaiming He, Bharath Hariharan, and Serge Belongie. Feature pyramid networks for object detection. In *CVPR*, 2017. 3
- [31] Tsung-Yi Lin, Priya Goyal, Ross Girshick, Kaiming He, and Piotr Dollár. Focal loss for dense object detection. In *ICCV*, 2017. 3
- [32] Tsung-Yi Lin, Michael Maire, Serge Belongie, James Hays, Pietro Perona, Deva Ramanan, Piotr Dollár, and C Lawrence Zitnick. Microsoft coco: Common objects in context. In *ECCV*, 2014. 1, 2, 3, 4, 5
- [33] Chenxi Liu, Liang-Chieh Chen, Florian Schroff, Hartwig Adam, Wei Hua, Alan L Yuille, and Li Fei-Fei. Auto-deeplab: Hierarchical neural architecture search for semantic image segmentation. In *CVPR*, 2019. 2
- [34] Shu Liu, Lu Qi, Haifang Qin, Jianping Shi, and Jiaya Jia. Path aggregation network for instance segmentation. In *CVPR*, 2018. 3
- [35] Ze Liu, Yutong Lin, Yue Cao, Han Hu, Yixuan Wei, Zheng Zhang, Stephen Lin, and Baining Guo. Swin transformer: Hierarchical vision transformer using shifted windows. In *Proceedings of the IEEE/CVF International Conference on Computer Vision*, 2021. 9
- [36] Jonathan Long, Evan Shelhamer, and Trevor Darrell. Fully convolutional networks for semantic segmentation. In *CVPR*, 2015. 2, 3
- [37] David Marr. *Vision: A computational investigation into the human representation and processing of visual information*. San Francisco: W.H. Freeman. Print., 1982. 4
- [38] Douglas Morrison, Adam W Tow, M McTaggart, R Smith, N Kelly-Boxall, S Wade-McCue, J Erskine, R Grinover, A Gurman, T Hunn, et al. Cartman: The low-cost cartesian manipulator that won the amazon robotics challenge. In *ICRA*, 2018. 2
- [39] Gerhard Neuhold, Tobias Ollmann, Samuel Rota Buló, and Peter Kotschieder. The mapillary vistas dataset for semantic understanding of street scenes. In *ICCV*, 2017. 3
- [40] Lu Qi, Li Jiang, Shu Liu, Xiaoyong Shen, and Jiaya Jia. Amodal instance segmentation with kins dataset. In *CVPR*, 2019. 2, 3
- [41] Lu Qi, Jason Kuen, Jiuxiang Gu, Zhe Lin, Yi Wang, Yukang Chen, Yanwei Li, and Jiaya Jia. Multi-scale aligned distillation for low-resolution detection. In *CVPR*, 2021. 3
- [42] Lu Qi, Jason Kuen, Yi Wang, Jiuxiang Gu, Hengshuang Zhao, Zhe Lin, Philip Torr, and Jiaya Jia. Open-world entity segmentation. *arXiv preprint arXiv:2107.14228*, 2021. 2, 5, 7
- [43] Stephan R Richter, Vibhav Vineet, Stefan Roth, and Vladlen Koltun. Playing for data: Ground truth from computer games. In *ECCV*, 2016. 3
- [44] Olga Russakovsky, Jia Deng, Hao Su, Jonathan Krause, Sanjeev Satheesh, Sean Ma, Zhiheng Huang, Andrej Karpathy, Aditya Khosla, Michael Bernstein, Alexander C. Berg, and Li Fei-Fei. ImageNet Large Scale Visual Recognition Challenge. *IJCV*, 2015. 5
- [45] Christoph Schuhmann, Richard Vencu, Romain Beaumont, Robert Kaczmarczyk, Clayton Mullis, Aarush Katta, Theo Coombes, Jenia Jitsev, and Aran Komatsuzaki. Laion-400m: Open dataset of clip-filtered 400 million image-text pairs. In *NeurIPS Workshop*, 2021. 3
- [46] Guang Shu. Human detection, tracking and segmentation in surveillance video. 2014. 2
- [47] Zhi Tian, Chunhua Shen, and Hao Chen. Conditional convolutions for instance segmentation. In *ECCV*, 2020. 3
- [48] Ashish Vaswani, Noam Shazeer, Niki Parmar, Jakob Uszkoreit, Llion Jones, Aidan N Gomez, Łukasz Kaiser, and Illia Polosukhin. Attention is all you need. In *NeurIPS*, 2017. 6
- [49] Huiyu Wang, Yukun Zhu, Hartwig Adam, Alan Yuille, and Liang-Chieh Chen. Max-deeplab: End-to-end panoptic segmentation with mask transformers. In *CVPR*, 2021. 3
- [50] Xinlong Wang, Tao Kong, Chunhua Shen, Yuning Jiang, and Lei Li. Solo: Segmenting objects by locations. In *ECCV*, 2020. 3
- [51] Yingqian Wang, Longguang Wang, Jungang Yang, Wei An, and Yulan Guo. Flickr1024: A large-scale dataset for stereo image super-resolution. In *ICCV Workshops*, 2019. 3
- [52] Magnus Wrenninge and Jonas Unger. Synscapes: A photorealistic synthetic dataset for street scene parsing. *arXiv preprint arXiv:1810.08705*, 2018. 3

- [53] Junfeng Wu, Yi Jiang, Song Bai, Wenqing Zhang, and Xiang Bai. Seqformer: Sequential transformer for video instance segmentation. In *ECCV*, 2022. 6
- [54] Yuxin Wu, Alexander Kirillov, Francisco Massa, Wan-Yen Lo, and Ross Girshick. Detectron2. <https://github.com/facebookresearch/detectron2>, 2019. 2
- [55] Gui-Song Xia, Xiang Bai, Jian Ding, Zhen Zhu, Serge Belongie, Jiebo Luo, Mihai Datcu, Marcello Pelillo, and Liangpei Zhang. Dots: A large-scale dataset for object detection in aerial images. In *CVPR*, 2018. 3
- [56] Yuwen Xiong, Renjie Liao, Hengshuang Zhao, Rui Hu, Min Bai, Ersin Yumer, and Raquel Urtasun. Upsnet: A unified panoptic segmentation network. In *CVPR*, 2019. 2
- [57] Hengshuang Zhao, Jianping Shi, Xiaojuan Qi, Xiaogang Wang, and Jiaya Jia. Pyramid scene parsing network. In *CVPR*, 2017. 2, 3
- [58] Hengshuang Zhao, Yi Zhang, Shu Liu, Jianping Shi, Chen Change Loy, Dahua Lin, and Jiaya Jia. Pscanet: Point-wise spatial attention network for scene parsing. In *ECCV*, 2018. 2
- [59] Jian Zhao, Jianshu Li, Yu Cheng, Terence Sim, Shuicheng Yan, and Jiashi Feng. Understanding humans in crowded scenes: Deep nested adversarial learning and a new benchmark for multi-human parsing. In *ACMMM*, 2018. 3
- [60] Bolei Zhou, Agata Lapedriza, Aditya Khosla, Aude Oliva, and Antonio Torralba. Places: A 10 million image database for scene recognition. *IEEE transactions on pattern analysis and machine intelligence*, 40(6):1452–1464, 2017. 3, 4
- [61] Bolei Zhou, Hang Zhao, Xavier Puig, Sanja Fidler, Adela Barriuso, and Antonio Torralba. Scene parsing through ade20k dataset. In *CVPR*, 2017. 1, 2, 3, 5
- [62] Yan Zhu, Yuandong Tian, Dimitris Metaxas, and Piotr Dollár. Semantic amodal segmentation. In *CVPR*, 2017. 3, 5